External-internal aerodynamic coupling on a turboprop engine using the Body-Force Method

Rocco Moretti, Julien Decours

EXTERNAL-INTERNAL AERODYNAMIC COUPLING ON A TURBOPROP ENGINE USING THE BODY-FORCE METHOD

Rocco MORETTI[1], Julien DECOURS[1]

[1]ONERA – The French Aerospace Lab, Université Paris Saclay, F-92190 Meudon, France

Abstract

This paper presents the work accomplished in the CleanSky2 ANTARES research project on the numerical simulation of the aerodynamics around the Tech TP turboprop demonstrator, including propeller and internal parts such as the air inlet and the first stage of Ardiden3 centrifugal compressor. Indeed, the internal and the external aerodynamics of an aeronautical engine are classically treated separately because of the different time scales and the different physical phenomena involved. The very different time scales make it unaffordable to simulate these two operating environments in the same simulation. In this work, the compressor has been modelled using the Body-Force Method (BFM) which allows us to overcome the time scale of the compressor, and therefore, to base the simulation on the largest time scale, i.e. that of the propeller. The performance of the compressor has been analyzed on the isolated and installed configuration. This work is a demonstration of the computational capacity that we have achieved within the project on this type of complex configurations.

Keywords: Body-Force, internal-external coupling, turboprop, centrifugal compressor, propeller

1 INTRODUCTION

With the advent of several innovative concepts and the continued need to make civil aviation more and more efficient and green, engine integration and its performance under distortion is being looked at in more detail. This is one of the goals of ANTARES [1], a project of the Clean Sky 2 research program. In particular, Safran Helicopter Engines and its partners (ONERA, MT-Propellers, NLR) have set up the Tech TP turboprop demonstrator (see Figure 1), which aims to study the benefits of using Ardiden 3 core engine to power a propeller-driven aircraft. The motivation for this project derives from the knowledge that turboprop engines offer better performance than turbojet engines in terms of fuel consumption and CO2 emissions. The Tech TP demonstrator aims to demonstrate at least 15% reduction in fuel consumption and CO2 emissions compared to turboprops currently in service, along with a reduction in noise emissions of at least 3 dBA [2].

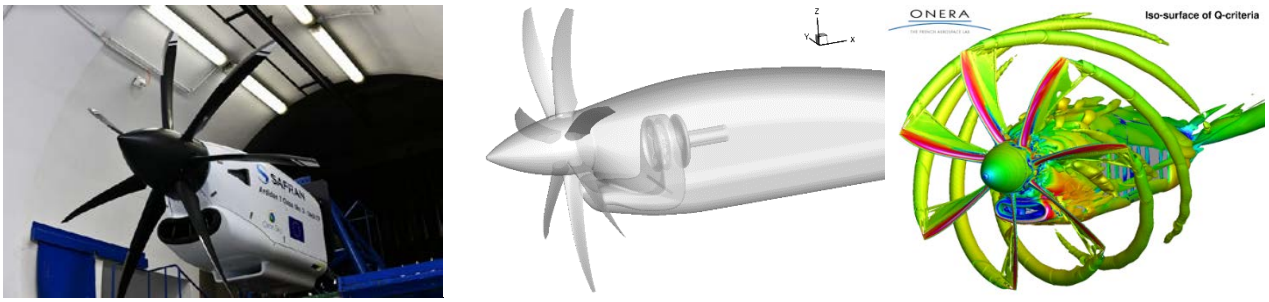

Figure 1 - Tech-TP demonstrator built in the CleanSky 2 ANTARES project. A photo of the test facility on the left, a visualization of the studied configuration on the center and a visualization of the Mach field on the right.

A first part of the ANTARES project was devoted to the design of the propeller. Three different designs were proposed by ONERA, MT-Propeller and NLR. The 7-blade propeller of ONERA was selected. Indeed, a numerical design process performed by ONERA allowed maintaining the

aerodynamic performance with a reduction of 5 dBA compared to the baseline 5-blade propeller proposed by MT-Propeller. The propeller was then manufactured by MT-Propeller and mounted on the Tech-TP demonstrator. A second part of the ANTARES project developped methodologies capable of simulating configurations such as a turboprop engine. Historically, the external and internal parts of an engine have always been treated separately. Nevertheless, in order to optimize an engine as much as possible, it has become essential to take into account the coupling between these two areas. Many studies have already been done on turbofan configurations. For example, it is the case for Ultra High Bypass Ratio (UHBR) turbofans set with short intakes [3] [4], integrated near the fuselage [5] or even within the fuselage [6] [7] [8] [9] [10] [11].

In a turboprop configuration, an additional complexity comes from the presence of the propeller. Indeed, the physics of the compressor and the propeller have very different characteristic times, i.e. the compressor rotates at a speed several tens of times higher than the propeller. Therefore, if we would like to simulate this type of configuration with the classical tools (URANS), it would be necessary to use the characteristic time of the compressor, which would be too small for the resolution of the physics of the propeller. This is why the simulation of this type of configuration is computationally costly today. Body-Force Methods (BFM) allow neglecting the characteristic time of the turbomachine by simulating only its steady behavior. The BFM has already been widely validated to simulate the behavior of a turbofan under distortion [12] [13] [14]. Nevertheless, publications on BFM for centrifugal compressors are scarcer [15] .

This paper aims to show a validation of the BFM on a centrifugal compressor under distortion and its application in a complex configuration like a turboprop, which to our knowledge has never been done in the literature. The paper consists in a brief description of the Body-Force method, a validation of the BFM on the isolated centrifugal compressor with/without distortion and the application of the BFM on the complete turboprop configuration.

2 METHODOLOGY

The approach used for the problem was to start from the simplest configuration, i.e. the isolated compressor, and to add progressively additional parts towards the complete configuration.

2.1 Body-Force Method

The body-force approach consists in replacing the bladed region by an axisymmetric volume where blockage, momentum and energy source terms are applied to each cell (see Figure 2).

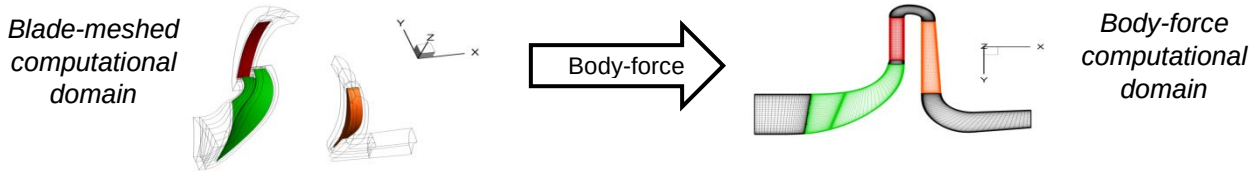

Figure 2 - Conversion of the computational domain with blades to BFM without blades.

Source terms are a combination of external data and flow proprieties so as to reproduce the effect of the blades on the flow. The following equation system presents the source terms applied in the right-hand side of the simplified Navier-Stokes equations:

$$\begin{cases} \frac{\partial \rho}{\partial t} + \operatorname{div}\left[\rho\left(\vec{v}-\vec{s}\right)\right] = S_b = \frac{\rho\vec{v}}{b}\cdot \vec{\operatorname{grad}}\left(b\right) & (1) \\ \frac{\partial \rho\vec{v}}{\partial t} + \vec{\operatorname{div}}\left[\rho\vec{v}\otimes\left(\vec{v}-\vec{s}\right)+p\vec{\vec{I}}-\vec{\vec{\tau}}\right] = S_b\vec{v}+\rho\vec{f} & (2) \\ \frac{\partial \rho e_t}{\partial t} + \operatorname{div}\left[\rho e_t\left(\vec{v}-\vec{s}\right)+p\vec{v}-\vec{\vec{\tau}}\cdot\vec{v}+\vec{q}\right] = S_b h_t + \rho r\Omega f_\theta & (3) \end{cases}$$

where $S_b = \frac{\rho\vec{v}}{b}\cdot\overrightarrow{grad}(b)$ models the blockage effects. b is the blockage factor (a geometrical

parameter) and ρ, $\vec{v}$ and h_t are respectively the local density, velocity field and stagnation specific enthalpy. Ω is the rotational speed and r is the radius.

In this work, the "body-forces" $\vec{f}$ were computed using the Hall's model [13]. In this formulation, $\vec{f}$ is decomposed in two components: $\overrightarrow{f_n}$ which is perpendicular to the flow relative velocity $\vec{w}$ and $\overrightarrow{f_p}$ which is parallel to $\vec{w}$. The first one reproduces the main deviation and the loading effects, while the second one models the losses because it is proportional to the entropy gradients. The Hall's formulation is defined by the following equations:

$$f_n = \frac{w^2}{2bh} 2\pi\delta \times \underbrace{\begin{cases} \frac{1}{\sqrt{1-M_{rel}{}^2}} & \text{if } M_{rel} < 1 \\ \\ \frac{4}{2\pi\sqrt{M_{rel}{}^2-1}} & \text{if } M_{rel} > 1 \end{cases}}_{\text{Compressible effects}^{14}} \tag{4}$$

$$f_p = \frac{w^2}{2bh} \left[K_{p0} + 2\pi \left(\delta - \delta_0 \right)^2 \right] \tag{5}$$

where M_{rel} is the relative Mach number, K_{p0} is the friction drag coefficient base on the local Reynolds number, δ is the flow local deviation in relation to the blade profile and δ_0 is the local deviation extracted from a computation at maximum efficiency operating point where only friction losses are applied.

The BFM allows to reduce the cost of the simulation thanks to the use of a lighter mesh (no meshed blades) but, above all, thanks to the possibility to perform a steady simulation since there are no rotating parts. On the other hand, the BFM neglects several secondary phenomena, such as blade wakes, corner separations or the tip-leakage flow [12] [14].

3 RESULTS

This section presents the results obtained in the ANTARES project. The Body-Force Method (BFM) has been validated for the isolated centrifugal compressor with and without inlet flow distortion. Then, the external aerodynamics has been added taking into account also the nacelle and the air inlet. Finally, the complete configuration has been simulated integrating the propeller through the Chimera (or overset grids) method.

3.1 ISOLATED COMPRESSOR

The BFM has been validated on three different iso-speed lines of the centrifugal compressor. Figure 3 shows one of the three iso-speed lines computed by the BFM and by the standard computation where blades are meshed. Figure 2 show the conversion from the initial mesh with blades to the BFM mesh which is meridian and have no blades.

The global behaviour of the compressor is well captured by the BFM, in particular near the maximum efficiency operating points. Towards blocking and surging, the gaps are larger because of the BFM's lack of ability to capture the secondary flows.

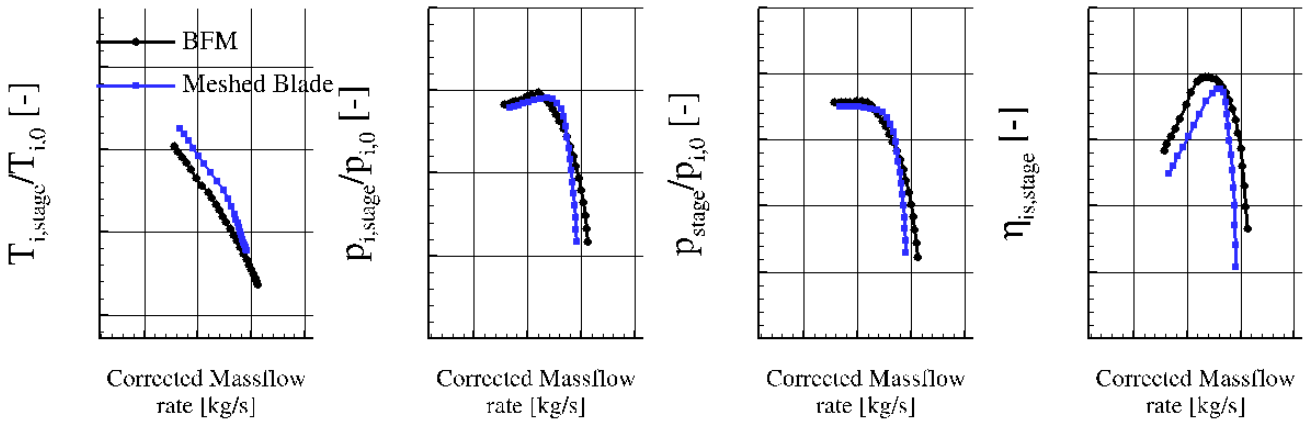

Figure 3 - Comparison of the 0D performances between the BFM results and the computation with the meshed blades for one of the three simulated rotation speeds.

3.2 ISOLATED COMPRESSOR WITH INLET DISTORTION

After validating the BFM on the isolated compressor with uniform injection, the problem was further complicated by injecting a fixed distortion. The distortion mapping has been extracted from the steady computation of the air-inlet configuration, as shown by Figure 4, and applied at the domain inlet for both BFM and URANS approaches.

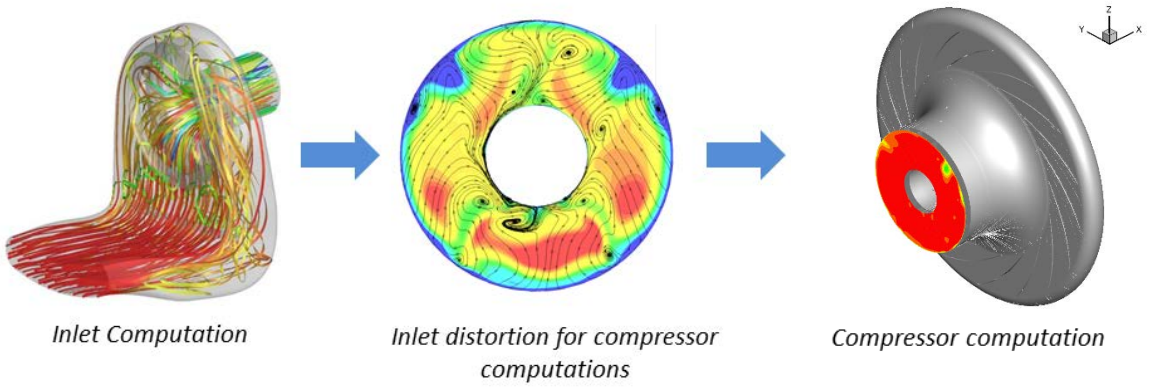

Figure 4 - Distortion mapping extraction (stagnation pressure) and its application to the compressor for the BFM and URANS blade meshed computations.

Figure 5 illustrates the impact of the inlet distortion on the compressor 0D performances evaluated by the BFM simulations.

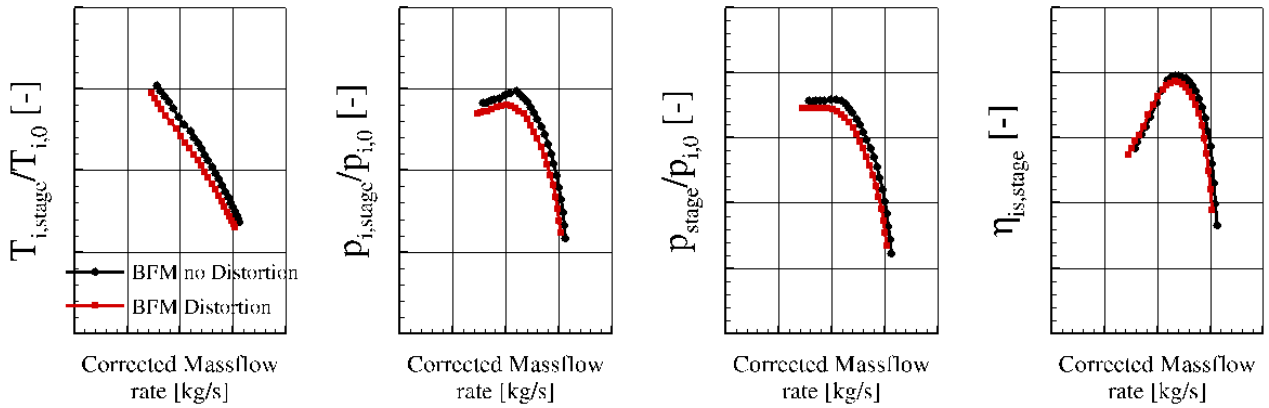

Figure 5 - Impact of the inlet distortion evaluated by the Body-Force approach on the 0D performances.

Table 1 shows the percentage loss in performance due to the distortion predicted by the BFM and the URANS. The percentage loss in performance computed by the BFM is in a good agreement with the URANS approach and the difference is acceptable for the iterative design process.

	$T_{i,stage}/T_{i,0}$	$p_{i,stage}/p_{i,0}$	$p_{stage}/p_{i,0}$	$\eta_{is,stage}$
BFM	-0.21%	-0.94%	-0.51%	-1.1pp
URANS	0.07%	-0.68%	-0.35%	-1.2pp

Table 1 - Distortion impact computed by BFM and URANS (in % or Percentage Point pp).

3.3 COMPLETE CONFIGURATION

Since the BFM has shown its ability to predict compressor performance with good accuracy even in the presence of distorted flow, the BFM has been included in the complete Tech TP demonstrator configuration including propeller, nacelle, air inlet and compressor. This configuration is shown in Figure 6.

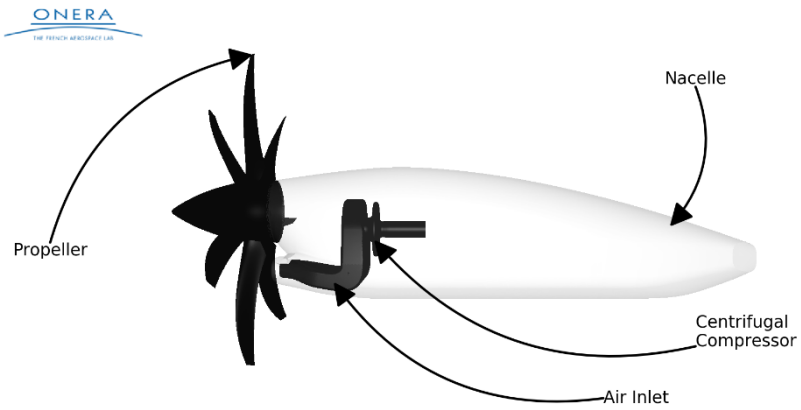

Figure 6 - Simulated configuration of the Tech TP demonstrator showing also the inside of the nacelle.

The propeller mesh was added into the complete configuration using the Chimera or overset grid approach (see Figure 7). The transfer of information between the compressor BFM mesh and the air inlet is achieved by mesh interpolation.

An outlet boundary condition is used at the outlet of the centrifugal compressor, and no air exhaust is modelled at the tail of the nacelle.

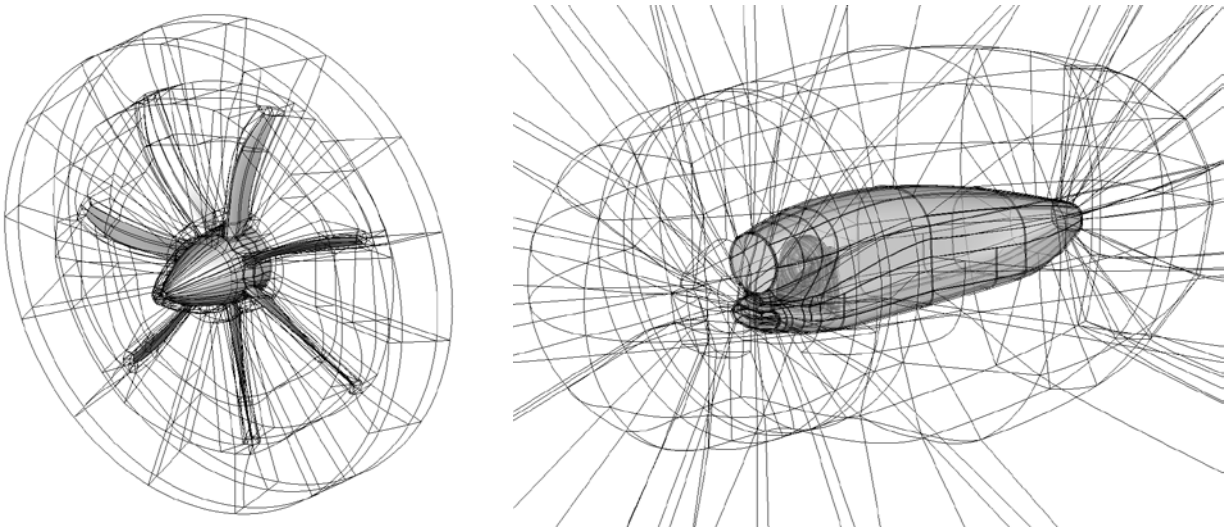

Figure 7 - Spinner and propeller mesh (left). Nacelle, inlet air, compressor and background mesh (right).

The resulting mesh has about 120 million cells. The computation was run on 463 cores (Intel Xeon « Cascade Lake - 6240R », 2.4 GHz, 35.75MB cache). It has been carried out with the elsA CFD software (v5.0.03) [16], which solves the Unsteady Reynolds Averaged Navier-Stokes (URANS) equations integrated by means of the finite volume approach. For the spatial discretisation, the Roe scheme is used and for the time integration the Gear method. The turbulence is modelled by the Smith model [17].

Thanks to the BFM, it was possible to neglect the compressor time scale and therefore to base the simulation on the time scale of the propeller. A physical time step corresponding to an azimuthal angle of 0.5° has been chosen for this computation. This allowed us to perform one revolution of the propeller in 12.5 hours. Few tens of propeller revolutions were necessary in order to have converged results.

Figure 8 shows the external flow of the turboprop. The momentum in the stream direction in the mid plane of the engine and the Q criterion are plotted. It is visible that the air inlet significantly disturbs the flow generated by the propeller. Indeed, a large separation is generated on the lips of the air inlet at each passage of a blade (visible by the periodicity of the momentum along the nacelle). From the graph located at the bottom of the image, displaying the thrust of a blade along its rotation, we can see that the maximum value is located right before the blade crosses the air inlet. This phenomenon is presumably due to air stagnation at the air inlet.

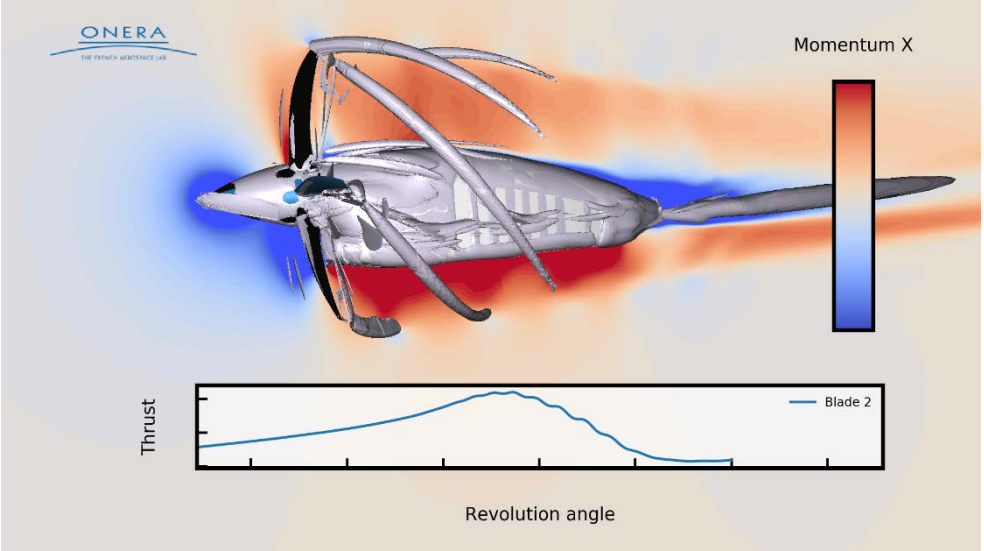

Figure 8 - Momentum field and Q-criterion of the complete configuration.

The internal flow is shown in Figure 9 and Figure 10. In Figure 9, the pressure field reveals the good behaviour of the Body-Force Method to simulate the centrifugal compressor, i.e. the pressure increase through the compressor. It is also interesting to notice the complex flow between the blade and the air inlet. This area remains sensitive despite the significant spinner improvement made during the project to reduce the separation at the beginning of the air inlet.

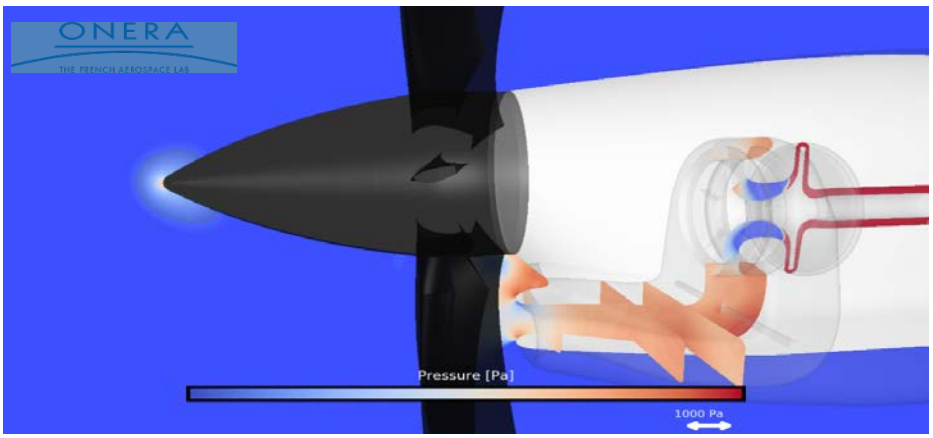

Figure 9 - Pressure field in the air inlet and in the compressor zone (figure aspect ratio deformed).

Figure 10 shows the Mach field in the mid-plane of the engine and on several slices across the width of the air inlet. The flow is largely slowed down by air inlet causing several detachments and stagnation zones in the corners and in the inner part of the air inlet. The resulting flow is complex and difficult to analyse. Indeed, the propeller disturbs the flow in the air inlet similar to an impulse at each blade passage.

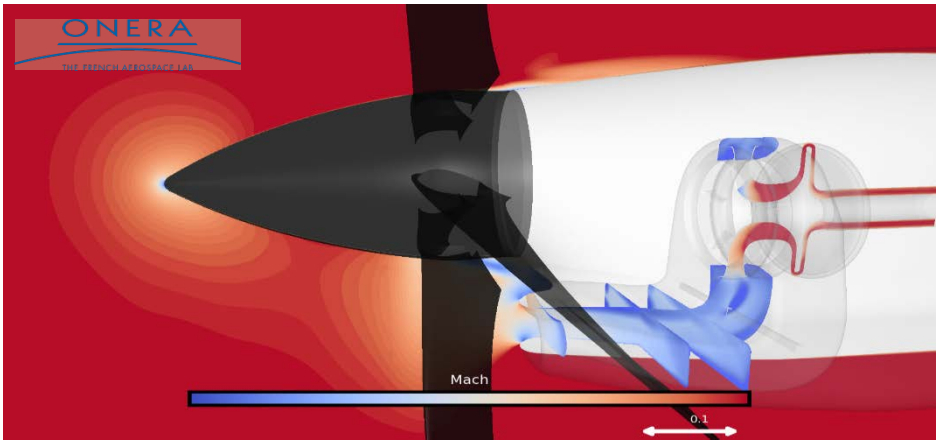

Figure 10 - Mach field in the air inlet (figure aspect ratio deformed).

This complex computation provides us with a good resolution of the flow at the compressor inlet. Figure 11 shows the distortion (in stagnation pressure) of the flow seen by the compressor at four instants of time. It is immediately apparent that the flow at the compressor inlet is unsteady and distorted due to the propeller and the air inlet perturbation. Indeed, the stagnation pressure can vary locally by several hundred Pascals.

This distorted flow will have a significant effect on the performance of the centrifugal compressor. For this purpose, the performance of the compressor was analysed.

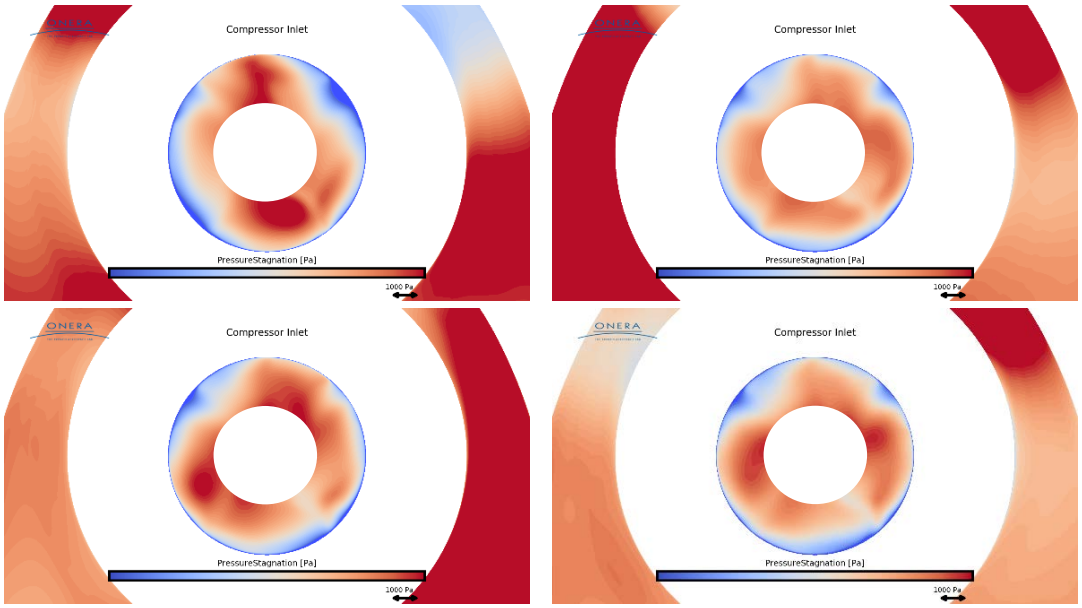

Figure 11 - Distortion in stagnation pressure at the compressor inlet at four different time instants (true inner radius of compressor not shown).

The analysis has been carried out on the time averaged flow field. The time used for the average is the time required for the propeller to complete one full revolution, because this is the period available with the finest time-step. Flow period is a function of the number of blades of the propeller, number of carter arms in the air inlet and number of blades of the compressor. Figure 12 compares the compressor performance map of the configuration including (green circle) or not (red diamond) the propeller with the performances computed on the isolated compressor. The blue line is the iso-speed line of the isolated compressor (though at operating conditions different from those of Figure 3) without distortion computed by the BFM and the black line is the one computed with the meshed blades.

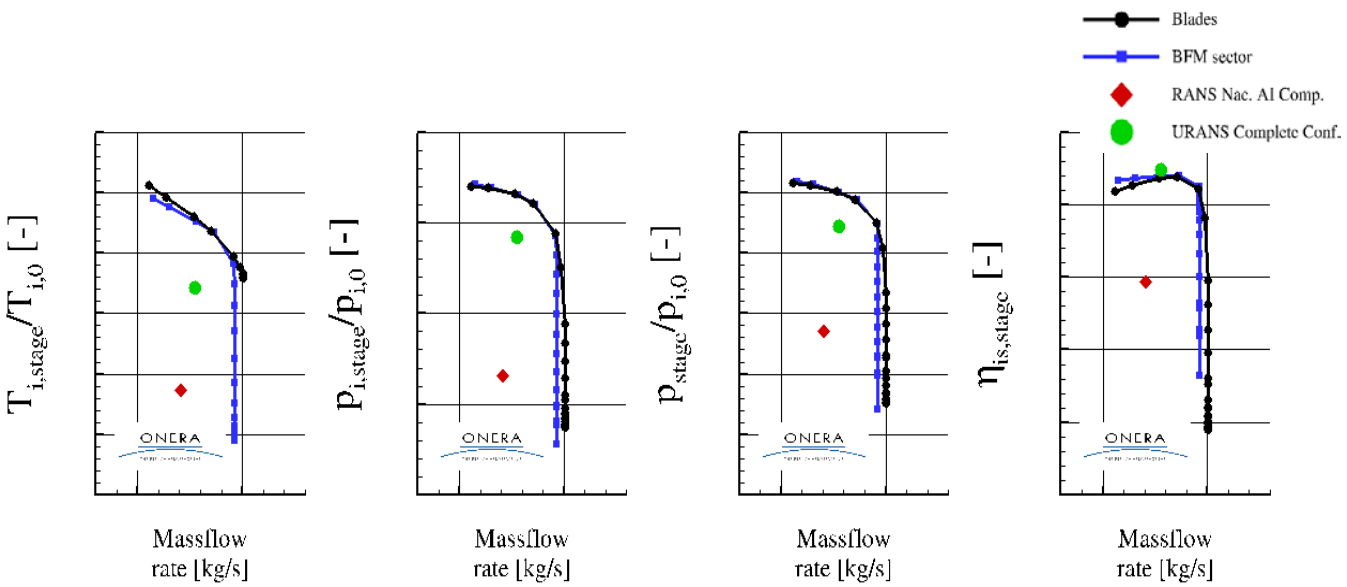

Figure 12 - Centrifugal compressor performance map of configuration with/without the propeller compared with the isolated compressor.

Safran Helicopter Engines provided the inlet condition used in the isolated compressor. This condition includes an empirical estimation of the air inlet losses -assuming an ideal inlet-, and does not account for the propeller effect.

The red diamond in Figure 12 corresponds to the compressor performance under distortion of the actual, solved, air inlet, but without propeller. The green dot includes the distortion from both the actual inlet and the propeller. According to the simulations done in this work, the propeller seems to compensate the losses introduced by the air inlet. Nonetheless special caution must be observed before drawing any conclusions.

A thorough analysis of the effects of propeller and air inlet on compressor performance requires comparing iso-speed lines and adjusting the operating conditions of the compressor. This work has focused on proposing a new simulation capability. Detailed performance analysis is out of the scope of this paper.

4 CONCLUSION

This paper shows the development of a methodology to study the aerodynamic interaction between the external and internal flow of a turboprop engine, where propeller and first centrifugal stage rotate at widely different speeds. This analysis, to our knowledge, has never been done in the literature before. This investigation was enabled by the Body-Force Method (BFM).

The authors would like to point out that this work was primarily a demonstration of the computational capability to simulate a complex configuration, such as a turboprop including the propeller, the nacelle, the air inlet and the first stage of the centrifugal compressor.

This work allowed showing the applicability of the Body-Force Method on a centrifugal compressor configuration under steady distortion and on a more complex, unsteady, configuration such as a turboprop. Regarding the centrifugal compressor application, although the BFM does not accurately assess the absolute value of engine performance, it captures the impact of distortions on performance quite well.

In the case of the turboprop application, the BFM makes it possible for us to carry out this type of simulation, which is currently unaffordable with conventional methods. In fact, this simulation allows us to directly evaluate the impact of unsteady phenomena that take place upstream of the compressor (propeller, nacelle, air inlet) on its performance. This new type of computation provides a powerful capability to assess accurately the aerodynamic distortion undergone by individual

components in the engine environment.

5 Acknowledgments

The authors would like to thank Safran Helicopter Engines colleagues for the very good, professional and fruitful cooperation. This work has been funded within the frame of the Joint Technology Initiative Clean Sky 2 ENGINES ITD (Integrated Technology Demonstrator) platform contract (Grant Agreement Number 945541 - GAM-2020-ENG) being part of the Horizon 2020 Research and Innovation framework program of the European Commission.

6 Contact Author Email Address

Mailto: rocco.moretti@onera.fr

7 Copyright Statement

8 References

[1] “CleanSky 2 : ANTARES project,” [Online]. Available: https://w3.onera.fr/antares/content/home. [Accessed 24 01 2022].

[2] “Tech TP : un démonstrateur qui a de l’avenir,” [Online]. Available: https://www.safran-group.com/fr/actualite/tech-tp-demonstrateur-qui-lavenir-2019-12-16. [Accessed 24 01 2022].

[3] A. Peters, *Ultra-Short Nacelles for Low Fan Pressure Ratio Propulsors,* PhD thesis, MIT, 2014.

[4] A. Peters, Z. S. Spakovszky, W. K. Lord and a. B. Rose, “Ultrashort nacelles for low fan pressure ratio propulsors,” *Journal of Turbomachinery,* vol. 137, 2014.

[5] H. Xie, Y. Wu, A. Wang and H. Ouyang, “Numerical investigation of inlet distortion for dfferent rear mounted engine installations at taking-off conditions,” in *ASME Turbo Expo 2015: Turbine Technical Conference and Exposition*, 2015.

[6] J. J. Defoe and Z. S. Spakovszky, “Effects of boundary-layer ingestion on the aero-acustics of transonic fan rotor,” *Journal of Turbomachinery,* vol. 135, no. 5, 2013.

[7] R. V. Florea, C. Matalanis, L. W. Hardin, M. Stucky and A. Shabbir., “Parametric analysis and design for embedded engine inlets,” *Journal of Propulsion and Power,* vol. 31, no. 3, 2015.

[8] L. Hardin, T. Tillman, O. P. Sharma, J. Berton and D. J. Arend., “Aircraft system study of boundary layer ingesting propulsion,” in *48th AIAA/ASME/SAE/ASEE Joint Propulsion Conference & Exhibit*, 2012.

[9] M.-S. Liou and B. J. Lee., “Minimizing inlet distortion for hybrid wing body aircraft,” *Journal of Turbomachinery,* vol. 134, no. 3, 2012.

[10] M.-F. Liou, H. Kim, B. Lee and M.-S. Liou., “Aerodynamic design of integrated propulsion-airframe configuration of the hybrid wing-body aircraft,” in *35th AIAA Applied Aerodynamics Conference*, 2017.

[11] A. Plas, M. Sargeant, V. Madani, D. Crichton, E. Greitzer, T. Hynes and C. Hall, “Performance of a boundary layer ingesting (bli) propulsion system,” in *45th American Institute of Aeronautics and Astronautics Aerospace Sciences Meeting and Exhibit*, Reno, NV, 2007.

[12] B. Godard, E. D. Jaeghere and N. Gourdain, “Effcient design investigation of a turbofan in distorted inlet conditions,” *Proceedings of ASME Turbo Expo 2019: Turbomachinery Technical Conference and Exposition,* no. GT2019-90471, 2019.

[13] D. K. Hall, “Analysis of civil aircraft propulsors with boundary layer ingestion,” PhD thesis, Massachusetts Institute of Technology, 2015.

[14] W. Thollet, G. Dufour, X. Carbonneau and F. Blanc, “Body-force modeling for aerodynamic analysis of air intake-fan interactions,” *International Journal of Numerical Methods for Heat & Fluid Flow,* vol. 26, no. 7, pp. 2018-2065, 2016.

[15] A. P. Kottapalli, “Development of a Body Force Model for Centrifugal Compressors,” Master of Science in Aeronautics and Astronautics, Massachusetts Institute of Technology, 2013.

[16] L. Cambier, S. Heib and S. Plot, “The Onera elsA CFD software : input from research and feedback from industry,,” *Mechanics & Industry,,* pp. 159-174, 2013.

[17] B. R. Smith, “The k-kL Turbulence Model and Wall Layer Model for Compressible Flows.,” in *AIAA 21st Fluid and Plasma Dynamics Conference*, Seattle, Washington, 1990.

[18] V. J. Fidalgo, C. Hall and Y. Colin., “A study of fan-distortion interaction within the nasa rotor 67 transonic stage.,” *Journal of Turbomachinery,* vol. 134, no. 5, 2012.